Journal of Environmental Chemical Engineering 13 (2025) 118907

Contents lists available at ScienceDirect

Journal of Environmental Chemical Engineering

journal homepage: www.elsevier.com/locate/jece

Advanced polystyrene nanoplastic remediation through electro-Fenton process: Degradation mechanisms and pathways

Qian Ye [a], Hao Xu [b], Timothy N. Hunter [c,*], David Harbottle [c], Girish M. Kale [c], Martin R. Tillotson [a,*]

[a] School of Civil Engineering, University of Leeds, Leeds LS2 9JT, UK
[b] Environment and Sustainability Institute, Faculty of Environment, Science and Economy, University of Exeter, Penryn TR10 9FE, UK
[c] School of Chemical and Process Engineering, University of Leeds, Leeds LS2 9JT, UK

ARTICLE INFO

Keywords:
Polystyrene
Electrochemical degradation
Nanoplastics
CuCo carbon aerogel
Degradation pathway

ABSTRACT

Nanoplastics are increasingly recognized as emerging pollutants posing significant ecological risks and necessitating the development of effective remediation strategies. Heterogeneous electro-Fenton (EF) processes have demonstrated excellent capabilities in degrading various persistent organic contaminants. Here, we propose a novel approach for the degradation of polystyrene nanoplastics (PS-NPs) by incorporating a copper-cobalt carbon aerogel (CuCo-CA) as a bifunctional cathode. The Cu/Co bimetallic pair was selected due to the complementary redox potentials of copper and cobalt, which can synergistically enhance the activation of H_2O_2, thus significantly improving catalytic efficiency. The bifunctional capability of CuCo-CA for H_2O_2 electro-synthesis and *in situ* activation induced the efficient generation of hydroxyl radicals for the oxidative decomposition of PS-NPs. Under optimized conditions (current: 20 mA, initial pH: 7.0, electrolyte 0.05 M, initial PS-NPs dosage: 20 mg/L), a PS-NPs removal efficiency of 94.8 % using UV-Vis spectroscopy, and total organic carbon removal of 73.7 % were achieved within 6 h. The CuCo-CA cathode maintained an excellent degradation rate and preserved active functional groups after five consecutive cycles. Characterization identified critical changes in morphology, particle size, composition, and functional groups of PS-NPs after electro-Fenton treatment. Density functional theory calculations were used to identify reactive sites on polystyrene, and the degradation pathways of PS-NPs were proposed for the first time. Analysis identified various chain-break and oxidation products, attributed to aggressive oxidative attack, while toxicity assessments confirmed that final products were substantially less harmful. Overall, this study addresses the critical environmental challenge of nanoplastics through an electro-Fenton system for sustainable remediation under mild conditions.

1. Introduction

Microplastics (MPs, 1 μm ~ 5 mm) and nanoplastics (NPs, < 1 μm) originate from ineffective or inappropriate plastics disposal in the environment and in-use degradation, e.g., from tires and textiles [1]. They are environmentally concerning due to their wide-ranging occurrence, small size, and resistant chemical properties [2]. These characteristics facilitate the entry of microplastics/nanoplastics (MPs/NPs) into animal and human bodies *via* food chains, affecting both aquatic life and human health through inhalation, ingestion, or direct contact [3]. Notably, nanoplastics may pose greater risks to the human digestive system and ecosystem compared to microplastics, due to their smaller particle size, larger surface area, and higher propensity for binding with other pollutants or reactive groups (–COOH, –NH_2) in the environment [4]. Approximately 1.5 million tons of MPs/NPs are estimated to be released into aquatic environments annually [5], prompting a need for innovative treatment solutions to tackle MPs and NPs pollution effectively.

Research on MPs/NPs separation in water primarily involves methods like filtration, sieving, and activated carbon, often used as pretreatment to quantify MPs/NPs [6]. However, these separation processes only achieve phase transfer of plastic particles. In contrast, decomposition techniques such as biological degradation and advanced oxidation processes (AOPs) facilitate the breakdown of chemical bonds within the MPs/NPs polymeric chain into smaller fragments or potentially mineralize to CO_2 and H_2O [7]. While researchers have discovered

* Corresponding authors.
E-mail addresses: T.N.Hunter@leeds.ac.uk (T.N. Hunter), M.R.Tillotson@leeds.ac.uk (M.R. Tillotson).

https://doi.org/10.1016/j.jece.2025.118907
Received 9 July 2025; Received in revised form 13 August 2025; Accepted 23 August 2025
Available online 24 August 2025
2213-3437/© 2025 The Authors. Published by Elsevier Ltd. This is an open access article under the CC BY license (http://creativecommons.org/licenses/by/4.0/).

that specific microorganisms, such as bacteria and fungi, are capable of degrading MPs/NPs [8], the practical application prospects of most reported biodegradation methods are limited by strict operating conditions and long processing times.

Recently, AOPs have demonstrated outstanding efficacy in degrading persistent organic contaminants in aqueous matrices through the generation of various reactive oxygen species (ROS), such as the hydroxyl radical (·OH) [9]. Nevertheless, the application of electrochemical advanced oxidation processes (EAOPs) for the removal/degradation of MPs/NPs in aquatic environments is still in its infancy. Electrooxidation (EO) processes employing boron-doped diamond (BDD) anodes and electrochemical oxidation systems featuring modified anodes, such as CeO_2-PbO_2, have shown higher degradation efficiencies for specific types of MPs [10]. Additionally, an electrooxidation-H_2O_2 system incorporating a BDD anode and carbon-felt cathode has been developed, significantly enhancing the degradation rate of polystyrene nanoparticles [11]. These early-stage studies indicated the great potential of EAOPs but also highlighted the need for further development [7].

The electro-Fenton (EF) process, one of the most effective and eco-friendly emerging technologies, is extensively reported for the degradation of various organic contaminants in water [12]. Although significant progress has been made in treating organic pollutants using EF processes, the application of these techniques for the removal of nanoplastics has been scarcely reported [7]. Limited studies have explored the mitigation of MPs/NPs pollution using EF or EF coupled with other techniques, such as the decomposition of PVC MPs using an electro-Fenton-like system equipped with a TiO_2/graphite cathode [13], and the effective decomposition of polystyrene NPs in a photoelectron-Fenton microreactor integrated with a MOF-derived porous α-Fe_2O_3 film [14]. Undoubtedly, the development of these methods offers highly advantageous degradation pathways for MPs and NPs. However, the reported EF system requires stringent reaction conditions, such as elevated temperatures of up to 100℃, to achieve a reduction in the weight loss of MPs. Additionally, the inclusion of irradiation in the photoelectron-Fenton process implies additional energy consumption and operational costs. Another reported electrochemical method relies on the addition of surfactants such as sodium dodecyl sulfate to achieve 40 % weight loss of MP in a relatively long treatment time (72 h) [15]. Consequently, there is an urgent need for highly efficient, cost-effective, and sustainable EF technologies to decompose micro/nano plastics from aquatic environments.

To explore the application of electro-Fenton technology in alleviating the nanoplastic crisis under mild conditions, this study proposes an electro-Fenton system with a copper-cobalt carbon aerogel (CuCo-CA) as an integrated cathode for treating polystyrene nanoplastics (PS-NPs), specifically to study the oxidative degradation mechanisms and environmental impact of intermediates. We have previously reported the decomposition of antibiotics using the CuCo-CA EF process and comprehensively studied the structural and electrochemical properties of the CuCo-CA cathode [16]. In addition, mechanisms of radical generation and electron transfer were detailed. Our findings showed that embedding Cu and Co into the carbon aerogel is beneficial due to the efficient redox cycling between Cu(I) and Cu(II), enabling rapid activation of H_2O_2, while Co(II) sites simultaneously promote additional generation of ·OH radicals. The conductive carbon matrix provides stabilization for these active sites, significantly enhancing catalytic stability and overall degradation efficiency. These previous results indicate that the CuCo-CA EF system has great potential to achieve plastic decomposition due to its strong oxidative ability and catalytic performance.

Polystyrene was selected as a representative nano-sized plastic because it is extensively utilized in foam products, cosmetics, and capacitor dielectrics, leading to its pervasive presence in aquatic environments [3]. The specific objectives of this research were to: (i) develop and optimize an electro-Fenton process for the degradation of polystyrene nanoplastics without reliance on external aeration; (ii) investigate the physical deformation and chemical composition alterations of PS-NPs during the electrochemical oxidation treatment; (iii) elucidate the underlying oxidation mechanisms and analyze the degradation pathways and intermediates of PS-NPs in an optimized EF process.

2. Experimental methods

Materials, chemicals, and more analytic methods are shown in Text S1 and Text S3 of Electronic Supplementary Material (ESM).

2.1. Electro-Fenton system construction based on CuCo-CA cathode

In this study, a CuCo-CA cathode was synthesized using the same method as in our previous study [16] and details are described in Text S2 of ESM. The prepared CuCo carbon aerogel (CuCo-CA) was employed directly as a bulk cathode material in the electro-Fenton system to degrade polystyrene nanoplastics. Degradation experiments for PS-NPs were conducted in a single-chamber cylindrical glass reactor at atmospheric pressure and ambient temperature, and a magnetic stirrer was used to evenly disperse the polystyrene nanoparticles. As shown in the schematic diagram (Figure S1), the cell consisted of a CuCo-CA cathode with an area of 4.5 cm^2 and a platinum sheet anode (4 cm^2), placed 2 cm apart. A DC power source (Velleman 70–0768) was adjusted to deliver an optimal current of 20 mA in most degradation processes, with the voltage ranging between 1.87 V and 2.6 V. To investigate the effect of different pH values, the initial pH of the electrolyte was controlled using 0.1 M H_2SO_4 and 0.1 M NaOH to attain the desired level. The reaction was initiated by introducing current into the electrolyte solution containing 0.05 M Na_2SO_4 and 20 mg/L of polystyrene. Samples were taken at specified intervals for analysis without filtration. The pH was measured using an HQ 40d (Hach, UK) digital multi-meter kit.

2.2. Characterization analysis

2.2.1. Polystyrene nanoplastics

The structural and size information of the polystyrene particles before and after electro-Fenton treatment was obtained using a high-resolution transmission electron microscope (HRTEM, FEI Titan3 Themis 300). A droplet of the aqueous suspension was applied onto a copper grid coated with a holey carbon film. Prior to any microscopic observation, the grids were hydrophilized through plasma treatment using a plasma cleaner (Henniker HPT-100). The surface morphological properties of PS-NPs were observed using a scanning electron microscope (SEM, Zeiss Evo 15). SEM images were acquired by depositing 10 μL of the PS-NPs onto an aluminum stub, which was covered with a silicon wafer and coated with a 5 nm layer of gold. The particle recognition and statistical size analysis were performed via Image J software (National Institutes of Health, USA). The size distribution and surface potential of nanoplastics within the pH range 3–9 were assessed on a Malvern Zetasizer ZS dynamic light-scattering (DLS) analyzer (Malvern Instruments Ltd., UK).

The chemical states of carbon and oxygen were analyzed using a Thermo Scientific K-Alpha X-ray photoelectron spectrometer (XPS). XPS analysis, including survey and high-resolution spectra, was conducted using an Al Kα radiation source operated at 10 mA and 15 kV, with a base pressure maintained at 2×10^{-9} mbar. The survey spectra were captured with an analyzer pass energy of 150 eV and an energy step size of 1.0 eV, while the high-resolution C 1 s and O 1 s spectra were collected at a pass energy of 50 eV with a step size of 0.1 eV. Energy calibration was conducted using the C 1 s peak of aliphatic carbon at 284.8 eV. The proportion of each component was determined by calculating the integrated area of each peak obtained from the fitting results. To further investigate the functional groups of the plastic particles, Fourier transform infrared spectroscopy (FTIR) analysis was carried out on both fresh and treated PS-NPs using a PerkinElmer Spectrum Two FTIR

spectrometer. Topographic images of PS-NPs particle arrangement and aggregation were obtained using an atomic force microscope (AFM, Bruker Innova), by dropping the particle suspension on a silicon wafer and then allowing it to dry naturally.

2.2.2. CuCo-CA cathode

To investigate any structural or compositional changes to the CuCo-CA cathode before and after recycling experiments, TEM, FTIR, and X-ray diffraction (XRD) analysis were conducted. Energy dispersive X-ray spectroscopy (EDS) mapping was executed using the same instrument employed for HRTEM with a HAADF detector. XRD analysis was carried out using a Shimadzu XRD-6100 instrument with Cu Kα radiation (λ = 1.5406 Å), scanning over a 2θ range of 10° to 80° with a step size of 0.02°. FTIR spectra over a wavelength range of 500–4000 cm^{-1} were acquired using a Nicolet iS5 spectrometer (Thermo Scientific) with KBr pellets.

2.3. Analytic methods

The determination of PS-NPs was conducted based on established methods from previous studies [17–19]. The concentration of PS-NPs was quantified using a UV-Vis spectrometer (Shimadzu UV1900) at 201 nm. A standard curve plotting absorbance versus concentration for PS-NPs was constructed across a concentration range of 0–20 mg/L, resulting in a correlation coefficient (R^2) of 0.9993 (Figure S2). The degradation of PS-NPs was modeled using a pseudo-first-order kinetic equation (Eq. 1), where C_0 denotes the initial PS-NPs concentration (mg/L), C_t represents the PS-NPs concentration at time t (mg/L), k_{obs} is the apparent rate constant (h^{-1}), and t is the reaction time (h).

$$\ln(C_0/C_t) = k_{obs}\, t \quad (1)$$

Total organic carbon (TOC) content in aqueous suspensions over the treatment period was evaluated using a Multi NC2100 (Analytik Jena) combustion analyzer. The measurements were performed on unfiltered samples, with 5 mL of the suspension collected at designated time intervals. TOC analysis does not directly quantify polymer concentrations in suspensions, but it provides insights into the conversion of organic carbon within polystyrene polymer into CO_2 during electrochemical oxidation. Specifically, the residual organic carbon in the suspension accounts for both the degradation intermediates resulting from partial decomposition of the PS-NPs and the remaining PS-NPs in the suspension.

Degradation intermediates of PS-NPs were analyzed by direct infusion mass spectrometry, which allowed rapid screening of key intermediates without risk of analyte loss by adsorption. Although direct infusion MS enables rapid screening of transformation products, it is subject to known limitations, such as ion suppression and the inability to resolve isomeric compounds. In this work, compound assignments were made based on accurate mass values, theoretical m/z calculations, and chemical plausibility within the expected degradation pathway.

2.4. Theoretical calculation

The density functional theory (DFT) computational calculations were carried out using the Gaussian 09 program package [20]. The B3LYP [21] density functional method with the D3(BJ) dispersion correction was employed to carry out all computations. The 6–31 G(d) basis set was used for the atoms in geometry optimizations, applying the PCM mode with water as the solvent. Vibrational frequency analyses at the same level of theory were performed to characterize stationary points as local minima without any imaginary frequencies. The Fukui function was employed to identify the reactive sites on the polystyrene (PS) molecule [22]. The condensed Fukui function was based on the natural charges of each atom (NPA). Further details on the DFT calculations are provided in Text S4.

3. Results and discussion

3.1. Analysis of polystyrene nanoplastic degradation performance in EF systems

3.1.1. Monitoring degradation performance using UV-Vis and TOC analysis

The reduction in UV-Vis absorbance in extracted samples served as an indicator for assessing the complete degradation progress of polystyrene nanoplastics (PS-NPs), and the efficiency of different electro-Fenton (EF) systems using copper-cobalt carbon aerogel (CuCo-CA), copper carbon aerogel (Cu-CA), cobalt carbon aerogel (Co-CA), and pure carbon aerogel (CA) as cathodes. As shown in Fig. 1(a), the EF process in the presence of the CuCo-CA cathode achieved the highest PS-NPs removal, reaching 94.8 % within 6 h, which may be attributed to enhanced generation of reactive species. The white reaction suspension of PS-NPs became clear and transparent following treatment with the CuCo-CA electro-Fenton system (Figure S3). In contrast, pure CA, without any transition metal loading, achieved 79.0 % removal that may be associated with the absence of catalytic metal sites. Additionally, Figure S4 and Fig. 1(b) present the pseudo-first-order kinetic fitting and rate constants for the different systems: 0.491 h^{-1} for CuCo-CA, 0.290 h^{-1} for Cu-CA, 0.426 h^{-1} for Co-CA, and 0.233 h^{-1} for pure CA. These highlight the synergistic effect of the Cu and Co bimetallic components on promoting PS-NPs decomposition through electro-Fenton mechanisms. TOC analysis was used as an independent quantitative verification for a complete PS-NPs breakdown. Although the TOC removal percentage was lower than that observed using UV-Vis removal, it reached 73.7 % after 6 h (Fig. 1(c)). The energy consumption (EC) of CuCo-CA EF process for PS-NPs degradation was evaluated according to Eq. 2. As shown in Table 1, the energy consumption of the established EF system to degrade PS-NPs was only 0.213 kWh $(gTOC)^{-1}$, which is beneficial in terms of energy efficiency. This suggests that a substantial proportion of the PS-NPs were gradually degraded and mineralized into CO_2 and H_2O through electrochemical oxidation, while a small portion remained in the reaction solution as intermediate breakdown products.

$$EC\ \left(kWh/g_{ToC}\right) = I * U * t\ \ /1000 * \Delta m_{TOC} \quad (2)$$

Where $EC\ (kWh/g_{TOC})$ is electricity consumption per g TOC removal, I is current (A), U is average voltage (V), t is reaction time (h), Δm_{TOC} is TOC removal (g).

Electro-Fenton systems typically induce oxidative degradation of organic pollutants by generating hydroxyl radicals (·OH, E_0 = 2.7 V versus normal hydrogen electrode [NHE]) as reactive oxygen species. Previous research by the current authors [23] demonstrated that ·OH serves as the dominant free radical in the EF process using a FeNi-CA cathode. Therefore, the concentration of ·OH generated in the CuCo-CA EF system over the reaction time was quantitatively analyzed using salicylic acid as a probe reagent. As shown in Fig. 1(d), after initiating the electro-Fenton reaction, ·OH radicals were continuously generated and gradually accumulated, reaching a maximum concentration of 175.3 μmol/L after 6 h. In our previous study on CuCo-CA EF system for tetracycline removal [16], because of the cooperative interaction between Cu and Co, the CuCo-CA cathode was shown to produce significantly more ·OH radicals than its monometallic counterparts (Cu-CA and Co-CA) and the metal-free carbon aerogel (CA). Under the same operating conditions, the H_2O_2 concentration in the CuCo-CA system rises to only ~10 μmol L^{-1} . The low steady-state H_2O_2 level despite the high ·OH yield confirms that electrogenerated H_2O_2 is rapidly activated by the Cu(I)/Cu(II)–Co(II)/Co(III) redox pair.

To further explore the role of ·OH species in the decomposition of PS-NPs using CuCo-CA as the cathode, a quenching test was conducted using tert-butanol (TBA) as a scavenger for ·OH [24]. As shown in Fig. 1 (a), the presence of TBA led to a decrease in PS-NPs removal from 93.6 % to 20.7 % after 6 h, highlighting the significant role of ·OH radicals in the degradation process. Residual removal (~20 %) in the

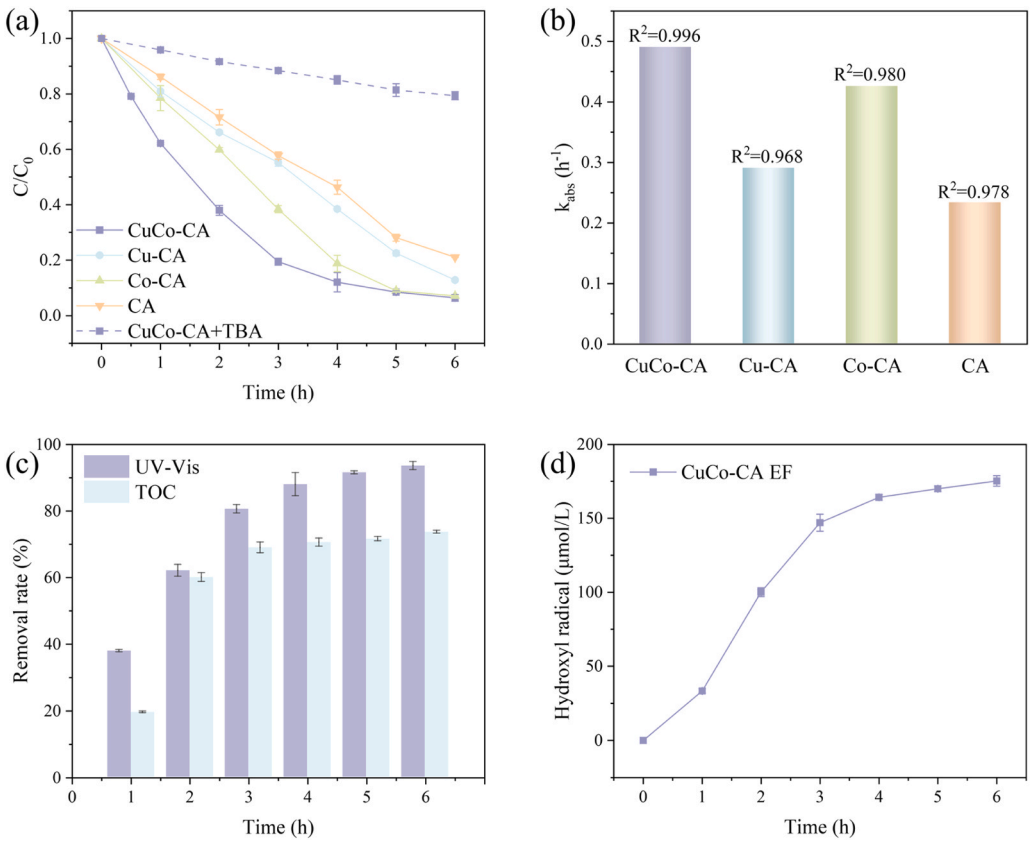

Fig. 1. (a) UV-Vis removal of PS-NPs in electro-Fenton systems using different cathodes, and impact of TBA; (b) Reaction rate constants of the pseudo-first-order kinetic model; (c) UV-Vis and TOC removal of PS-NPs in the CuCo-CA EF system; and (d) Generation of hydroxyl radicals in the CuCo-CA EF system. Conditions: [PS-NPs] = 20 mg/L, pH 7.0, applied current 20 mA, [Na_2SO_4] = 0.05 mol/L, [salicylic acid] = 0.01 M, [TBA] = 1 M, no aeration.

Table 1
Energy consumption (EC) for PS-NPs degradation in CuCo-CA EF system. Conditions: pH_0-7.0, Na_2SO_4-50 mM, PS-NPs-20 mg/L, 20 mA.

I(A)	$U_{average}$(V)	t (h)	ΔTOC (mg/L)	Volume (L)	Δm_{TOC}(g)	EC (kWh/g_{TOC})
0.02	2.235	6	8.4	0.15	1.26×10^{-3}	0.213

presence of TBA may be attributed to superoxide radicals ($\cdot O_2^-$) detected in our earlier work on CuCo-CA by DMPO–OOH Electron-Spin Resonance (ESR) signals [16]. Although less reactive than ·OH, $\cdot O_2^-$ can attack oxidized polymer chains and thus contributes to PS-NPs degradation.

3.1.2. *Optimization of operational parameters*

To optimize reaction conditions in the CuCo-CA EF system, operational parameters (i.e., initial pH, current, PS-NPs concentration, and electrolyte concentration) affecting the removal of PS-NPs were further investigated in Fig. 2. The pseudo-first-order kinetic fitting and reaction rate constant under each parameter are shown in Figure S5 and Fig. 3, respectively. The pH condition played a vital role in influencing the efficacy of the heterogeneous electro-Fenton system, as it impacts the speciation of pollutants and electrochemical reactions. In acidic solutions, the increased availability of protons facilitated the conversion of dissolved oxygen into H_2O_2 *via* a two-electron pathway, as described by Eq. 3 [25]. Although a high decrease in apparent UV-Vis absorbance was observed at pH 3, this was mainly attributed to the effect of adsorption between PS-NPs and CuCo-CA cathode rather than actual oxidative degradation (Fig. 2(a)). At other pH values, the contribution of adsorption to the degradation rate was almost negligible. The PS-NPs possess a mildly negative surface charge due to the presence of sodium dodecyl benzene sulfonate (SDBS), a common surfactant. This gives rise to electrostatic interactions as a key driver in adsorption. The CuCo-CA electrode surface contains functional groups such as –OH and –COOH (as confirmed by FTIR spectra in Section 3.1.3), whose protonation state depends on the solution pH. At low pH, these groups tend to be protonated, resulting in a positively charged surface. At high pH, deprotonation leads to a negatively charged surface [26]. Thus, the significantly enhanced adsorption of PS-NPs at pH 3 is likely due to strong electrostatic attraction between the negatively charged nanoplastics and the positively charged CuCo-CA surface under acidic conditions. In contrast, at higher pH values, electrostatic repulsion and higher particle stability reduce physical adsorption.

Additionally, the increase in pH helped to reduce the oxidation potential of ·OH radicals, thereby lowering the threshold for ·OH generation [27]. This may explain the 80 % removal efficiency observed under pH 9 condition. Overall, in the initial pH range of 3–9, removal efficiencies ranged from 69 % to 94 % for the CuCo-CA EF system over 6 h. The optimal operational pH condition for PS-NPs removal in the CuCo-CA EF system was pH 7, and the peak reaction rate constant (0.491 h^{-1}) was attained at pH 7.0, as shown in Fig. 3.

$$\text{Cathode}: \quad O_2 + 2H^+ + 2e^- \rightarrow \quad H_2O_2 \tag{3}$$

The efficacy of EF systems was significantly influenced by the applied current density, which drove electron transfer and correlated with the rate of H_2O_2 production. A higher current density increased the quantity of ·OH radicals both in solution and physisorbed on the electrodes [25]; thus, the PS-NPs removal efficiency after 6 h improved from 85 % to 94 % as the current rose from 10 mA to 20 mA (Fig. 2(b)). The quantitative measurements of ·OH radical concentrations under various applied currents (Figure S6) also show that moderate current enhances

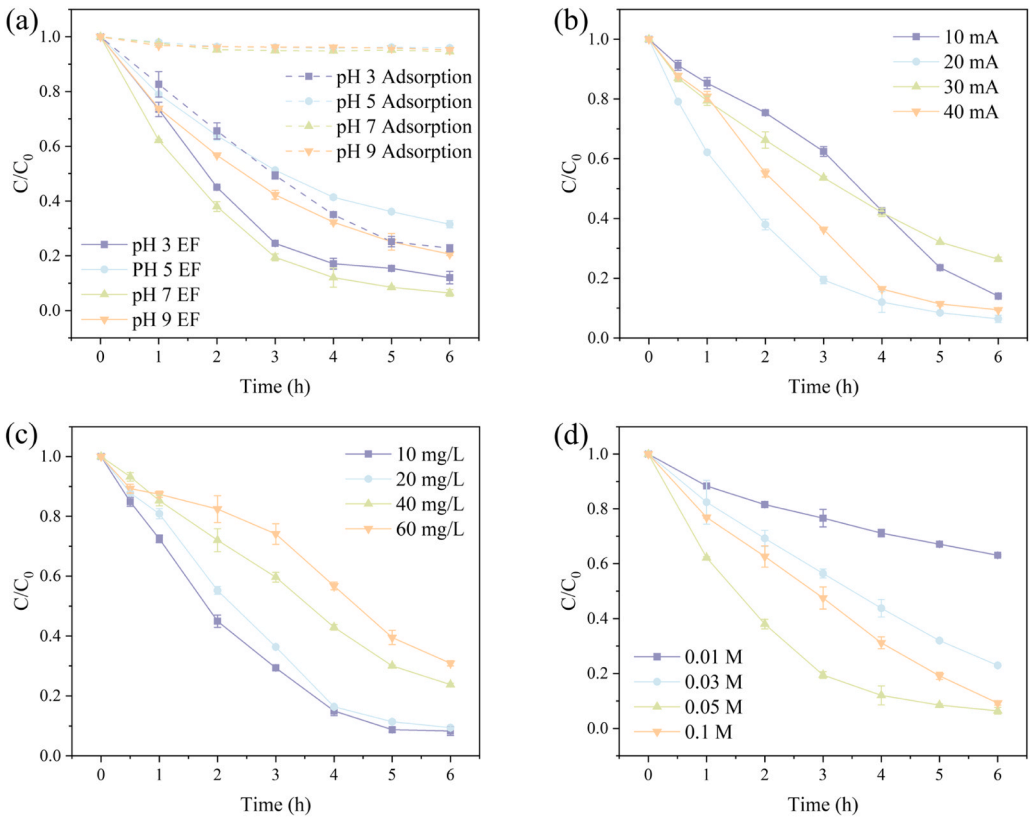

Fig. 2. Impact of (a) initial pH value; (b) current; (c) initial concentration of PS-NPs; and (d) Na_2SO_4 concentration on PS-NPs removal in the CuCo-CA EF system.

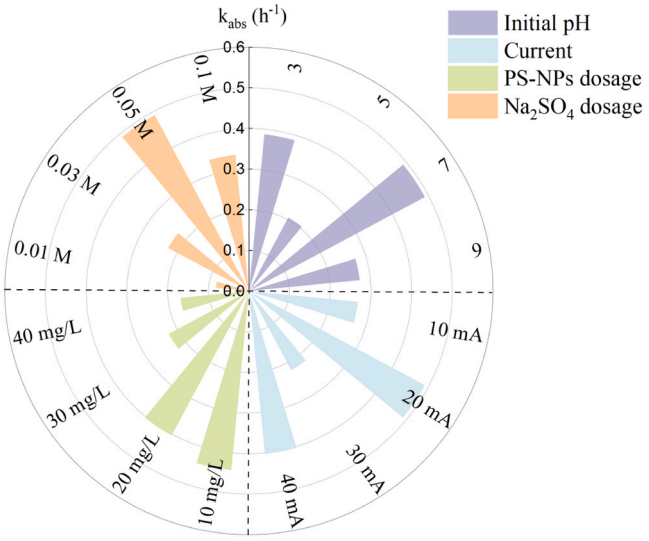

Fig. 3. Reaction rate constant comparison under various conditions.

the $2e^-$ ORR process for H_2O_2 production, which in turn increases ·OH through the Fenton-like reaction. However, a drop in reaction rate was observed when the applied current was increased to 30 mA and 40 mA, since high applied current densities enhanced the rate of side reactions, including cathodic hydrogen evolution (Eq. 4) and parasitic reactions, involving ·OH radicals (Eq. 5) [28]. At higher currents, the cathode potential becomes sufficiently negative to promote hydrogen evolution (HER), which competes with O_2 reduction and reduces H_2O_2/·OH formation efficiency. Simultaneously, higher ·OH concentrations can increase the rate of radical-radical recombination, further reducing available oxidants. Therefore, the optimal applied current in the CuCo-CA EF system for PS-NPs removal was 20 mA to balance radical production and energy efficiency.

$$2H^+ + 2e^- \rightarrow H_2 \quad (4)$$

$$2 \bullet OH \rightarrow O_2 + 2H^+ + 2e^- \quad (5)$$

As shown in Fig. 2(c), overall degradation efficiency showed a slight difference between the initial PS-NPs concentrations of 10 mg/L and 20 mg/L, with over 90 % PS-NPs removal observed under these conditions. Additional increases in PS-NPs concentration beyond a particular threshold of 20 mg/L led to a decrease in removal efficiency, although it would be expected that similar removal end-points may be achieved over longer periods than studied. This phenomenon may be attributed to the fact that under specific reaction conditions, a finite amount of ·OH radicals is generated per unit time. When the pollutant concentration increased, the available ·OH radicals became insufficient to effectively degrade the elevated levels of pollutant, resulting in a decrease in pollutant removal rate. This observation has been noted by other researchers [29,30].

Sodium sulfate (Na_2SO_4) is widely used as an electrolyte in EF processes due to its high ionic strength and minimal interference in aqueous solution [25], and its concentration plays a critical role in reaction efficiency. Low electrolyte concentrations may not provide sufficient conductivity, while high concentrations can lead to electrode corrosion and reduce the reaction time of Fenton reagents [31]. The removal efficiency of polystyrene particles increased from 37.0 % at 0.01 M Na_2SO_4 to 93.6 % at an optimal concentration of 0.05 M Na_2SO_4 (Fig. 2 (d)), and the reaction rate constant improved from 0.082 h^{-1} to 0.491 h^{-1} (Fig. 3). However, when Na_2SO_4 dosage was further increased to 0.1 M, removal efficiency significantly decreased, likely due to SO_4^{2-} ions consuming radicals (Eq. 6 and Eq. 7) [25].

$$\bullet OH + SO_4^{2-} \rightarrow OH^- + \bullet SO_4^- \quad (6)$$

$$\bullet SO_4^- + e^- \rightarrow SO_4^{2-} \quad (7)$$

3.1.3. Reusability and stability of the CuCo-CA cathode

The recycling performance of the cathode material helps determine the economic benefit of the treatment process. After cleaning and drying, the CuCo-CA cathode was applied to the EF system for five consecutive runs, and the degradation of PS-NPs under identical reaction parameters is shown in Fig. 4(a). The results indicated a slight decline in PS-NPs removal efficiency after five consecutive cycles and 6 h reaction time. The reusability performance of the CuCo-CA cathode was greatly influenced by its structural characteristics; hence, the microstructural features of the CuCo-CA cathode were further investigated. As shown in the TEM images (Fig. 4(d)~(e)), uniformly distributed CuCo nanoparticles formed within the carbon matrix, where the presence of transition metals catalyzed the formation of graphitic carbon, thereby enhancing conductivity and facilitating electron transfer. EDS mapping was executed to reveal the element distribution (Figure S7). In the selected field, elemental C presents a uniform, high-intensity signal over the entire field, which confirms the continuous carbon aerogel backbone. Elemental O shows a weak, diffuse background with slightly brighter spots coincident with Cu/Co, indicating surface-bound -OH/-O- as well as thin Cu- or Co-oxide shells formed during air exposure. The Cu and Co signals overlap the carbon skeleton, indicating that metals are embedded or strongly anchored rather than merely physisorbed, which helps suppress metal leaching in long-term runs.

Fig. 4(b)~(c) show the lattice structure and functional group changes of the cathode before and after reuse. XRD spectra revealed that catalytically active Cu(I) species were oxidized to Cu(II) during the reaction, activating H_2O_2 to produce ·OH radicals (Eq. 8) [32]. However, the catalytic performance of such a Cu-based system is closely tied to the redox cycling between Cu(I) and Cu(II). Cu(I) rapidly reacts with H_2O_2 ($k = 4.7 \times 10^3\ M^{-1}\ s^{-1}$) to generate ·OH radicals whereas Cu(II) exhibits a much lower rate ($k = 460\ M^{-1}\ s^{-1}$) and yields less reactive ·OOH species ($Cu^{2+} + H_2O_2 \rightarrow Cu^+ + H^+ + \cdot OOH$) [33]. The progressive oxidation of Cu(I) to Cu(II) during operation can hinder the redox cycling necessary for efficient H_2O_2 activation, potentially leading to the slight decline in PS-NPs removal efficiency. To address this, electrochemical methods such as periodic potential pulsing may be used to maintain the catalytic activity of Cu-based electrode due to the process of regeneration and stabilization of the Cu oxidation state [34]. In addition, mild chemical reducing agents (such as ascorbic acid) may also regenerate Cu(I) without affecting the structure of the carbon material [35].

XRD results show that the graphitic carbon matrix and the Cu/Co phases are preserved after five cycles. Besides, FTIR analysis showed oxygen functional groups such as -OH and -COO- groups remained after reuse. Our earlier work [16] indicates that graphitic carbon functions as an electron transport framework while Cu and Co metal sites catalyze the in situ activation of H_2O_2 to produce reactive radicals. In addition, oxygen functional groups played a crucial role in the electrosynthesis process of H_2O_2 [36], indicating that the cathode retains its electrocatalytic activity for $2e^-$ ORR. Consequently, long-term EF performance relies on the cooperative action of (i) surface oxygen groups that drive $2e^-$ ORR, (ii) Cu/Co sites that activate H_2O_2, and (iii) the conductive graphitic framework that supports rapid electron transfer. The CuCo-CA cathode therefore demonstrated structural stability and recyclability during the oxidative degradation of PS-NPs, highlighting its potential for application in water purification to address nanoplastic contamination.

$$Cu(I) + H_2O_2 \rightarrow Cu(II) + \bullet OH + OH^- \quad (8)$$

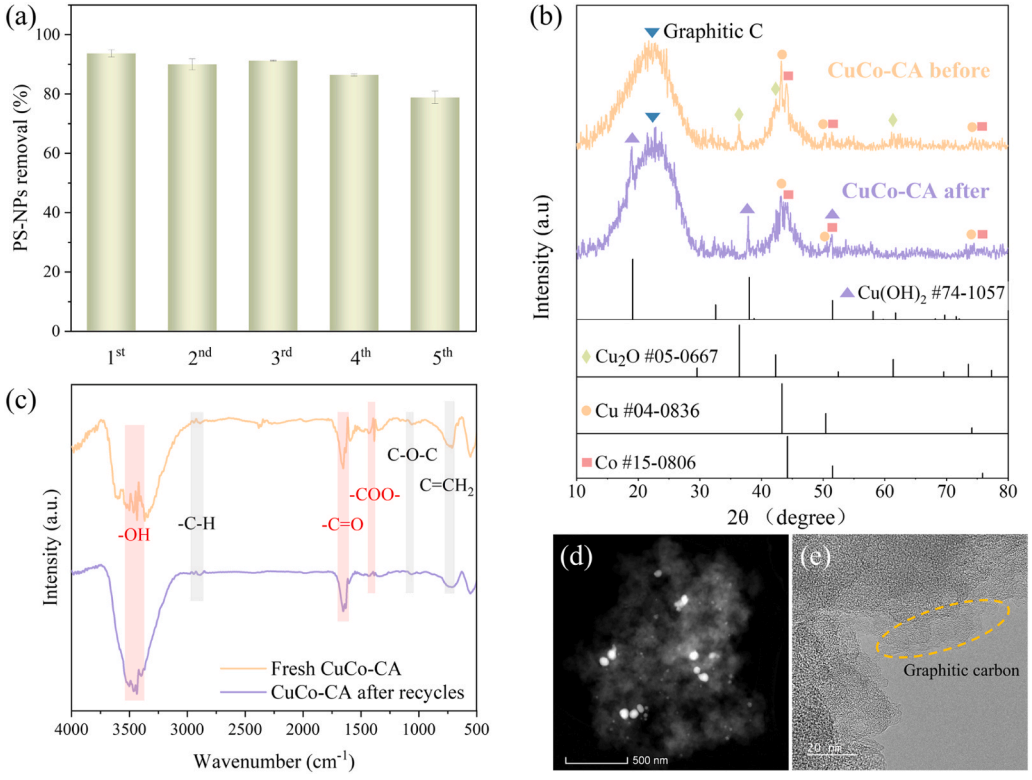

Fig. 4. (a) Recycling performance of the CuCo-CA cathode on PS-NPs removal; (b) XRD spectrum and (c) FTIR spectrum of the CuCo-CA cathode before and after recycling; (d) and (e) HRTEM images of the original CuCo-CA cathode. Conditions: [PS-NPs] = 20 mg/L, pH 7.0, applied current = 20 mA, [Na_2SO_4] = 0.05 mol/L, no aeration.

3.2. Investigation of structural and compositional changes to PS-NPs

3.2.1. Zeta potential, SEM/TEM imaging, and dynamic light scattering analysis

Zeta potential measurements were conducted across varying pH levels to gain insights into PS-NPs dispersion stability. As shown in Fig. 5 (a), the zeta potential of the nanoparticles generally varied between −15 mV and −40 mV with increasing pH. The negative charge observed on PS-NPs across the entire pH range may be attributed to the anionic charge derived from sodium dodecyl benzene sulfonate present on the nanoparticles, which was added to control the particle size during synthesis and to prevent agglomeration during storage. A zeta potential value of approximately −30 mV at pH 7 suggests the PS-NPs are electrostatically stable and well-dispersed as colloids [18]. Dynamic light scattering (DLS) was applied to measure the size distribution of PS-NPs before and after treatment in the CuCo-CA EF process, Fig. 5(b). The intensity-based particle size distribution of PS-NPs before the reaction, measured at pH 7 and 25℃, indicated a particle size of approximately 120 nm, consistent with the size observed in SEM imaging (Fig. 5(c)). While the intensity of the pre-reaction peak centered at around 120 nm diminished after treatment, the DLS measurements indicated the emergence of larger particles, as well as a broadening of the distribution post-treatment. This phenomenon may be attributed to PS-NPs particle aggregation, which could be influenced by changes in pH during the reaction (e.g., pH decreased from 7.0 to 3.2 after 6 h degradation) and modifications to the surface functional groups of the polymer nanobeads during the reaction. It is also clear, therefore, that complete degradation of the PS-NPs is not achieved (as inferred from TOC analysis), with residual PS-NPs being unstable in their partially degraded state.

Transmission electron microscope (TEM) is an intuitive technique for visually assessing particle alterations during oxidative treatment, allowing for a quantitative analysis through statistical evaluation of nanoparticle size distribution. Fig. 6(a1)~(a2) indicates that the fresh PS-NPs exhibited a smooth, spherical morphology with distinct edges and a uniform particle size distribution. The mean diameter of the fresh PS-NPs was 118.6 nm, which aligned with the size distribution results from DLS analysis. The fading of particle boundaries and the presence of polymeric fragments were observed following electrochemical treatment, Fig. 6(b1) and Fig. 6(c)~(f). It may be inferred that new surface functional groups formed as a result of polymer chain breakdown during the radical attack, leading to a loss of spherical definition and particle agglomeration due to surface adhesion [37]. Additionally, a particle size reduction was clearly evidenced through statistical analysis of mean diameter, Fig. 6(b2). Critically, the TEM therefore suggests that electrochemical treatment results in evolving surface degradation that breaks down the PS-NPs from the outside in. It is also noted that in the focal resolution of the TEM, it was not possible to observe the larger particle clusters measured from the DLS, while it is emphasised that the TEM images post-treatment only capture the small overall fraction of particles that remain. It is still assumed that the great majority of particles are fully degraded and removed from the system.

3.2.2. XPS, FTIR, and AFM analysis

The structural and functional group changes to the polystyrene nanoplastics (PS-NPs) during CuCo-CA EF system treatment were characterized using Fourier Transform Infrared Spectroscopy (FTIR, Fig. 7 (a)). The aromatic C-H stretch vibrations at 3060 and 3026 cm^{-1}, along with the $–CH_2$ asymmetric stretch vibration at 2924 cm^{-1}, represent typical absorption bands of polystyrene [38]. The characteristic absorption bands of the benzene ring were observed at 1601 and 1493 cm^{-1}, which may be associated with the stretching modes of C═C bonds [39]. The spectral bands at around 697 cm^{-1}, 756 cm^{-1}, 906 cm^{-1}, and 1028 cm^{-1} were indicative of C-H out-of-plane vibrations, suggesting the presence of a single substituent on the aromatic benzene ring and confirming the characteristic phenyl ring structure of polystyrene [40]. The distinct functional groups of PS-NPs (i.e., cyclic C-H and C═C bonds) remained stable after EF treatment. However, oxidative degradation is known to induce changes in surface functional groups, particularly in the carbonyl region (1650–1850 cm^{-1}) [41], which were observed in the zoomed spectra, Fig. 7(a). The FTIR results demonstrated the incorporation of carbonyl groups such as carboxylic acids, aldehydes, esters, and ketones onto the PS-NPs surface because of electrochemical oxidation processes.

Fig. 7(b) presents the X-ray photoelectron spectrometer (XPS) survey spectra of the original PS-NPs and PS-NPs with the EF process after 6 h. The original PS-NPs exhibited C 1 s and O 1 s peaks, with atomic percentages of 98.8 % and 1.2 %, respectively. In contrast, after 6 h of electrochemical oxidation, the oxygen content in the PS-NPs increased to 4.9 %. This rise in the O/C ratio might be attributed to rapid oxidation on the surface under attack from free radicals [42]. Additionally, the C 1 s peaks in Fig. 7(c) were deconvoluted into three main components, corresponding to C-C/C-H (284.8 eV), C-OH/C-O-C (286.14 eV), and π-π* bonding (291.5 eV) [43,44]. Following EF treatment with the CuCo-CA cathode, there was a notable increase in the C-OH/C-O-C content, while the peak area of C-C/C-H decreased after oxidation. The π-π* intensity, a signature feature of phenyl rings, showed a slight reduction following 6 h of EF treatment. This decline could be caused by either the cleavage of phenyl rings or the release of small phenyl-containing molecules from the polystyrene structure. [42]. In the O 1 s spectra of PS-NPs, Fig. 7(d), peaks corresponding to C═O (532.26 eV), C-O (533.01 eV), COOH (533.85 eV), and O═C-O-O (535.28 eV) [45] were observed in both pre- and post-reaction samples. The increased intensity of oxygen atoms and oxygen-containing functional groups on the PS-NPs surface indicated oxidation had occurred during treatment. Notably, the number of C-O groups in the PS-NPs increased from 37.9 % to 42.1 % after 6 h oxidation, consistent with the findings from the C 1 s high-resolution spectrum. Based on the FTIR results (Fig. 7(a)), the incorporation of carbonyl groups onto the surface

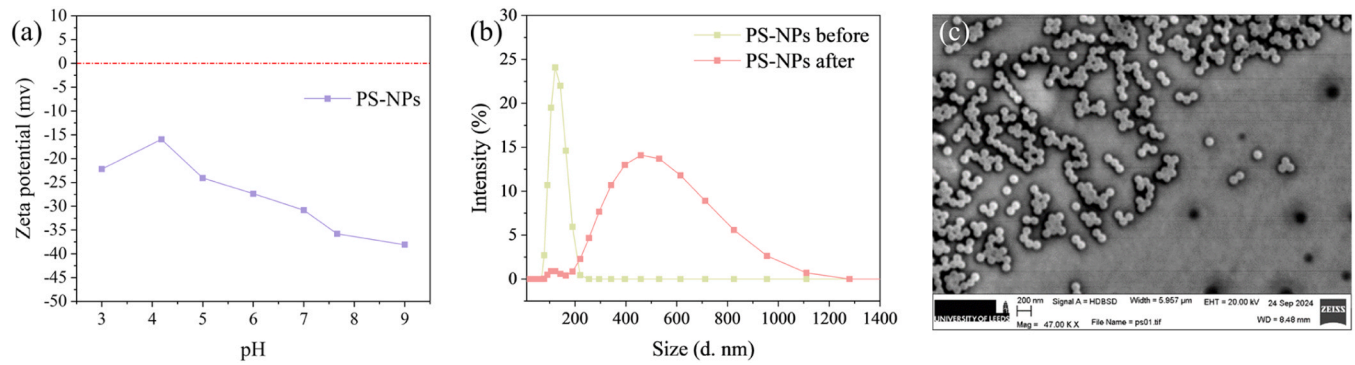

Fig. 5. (a) Zeta potential under different pH conditions of original PS-NPs; (b) Dynamic light-scattering size distribution of PS-NPs before and after EF reaction; and (c) SEM images of original PS-NPs. Conditions: [PS-NPs] = 20 mg/L, pH 7.0, Applied current = 20 mA, [Na_2SO_4] = 0.05 mol/L, no aeration.

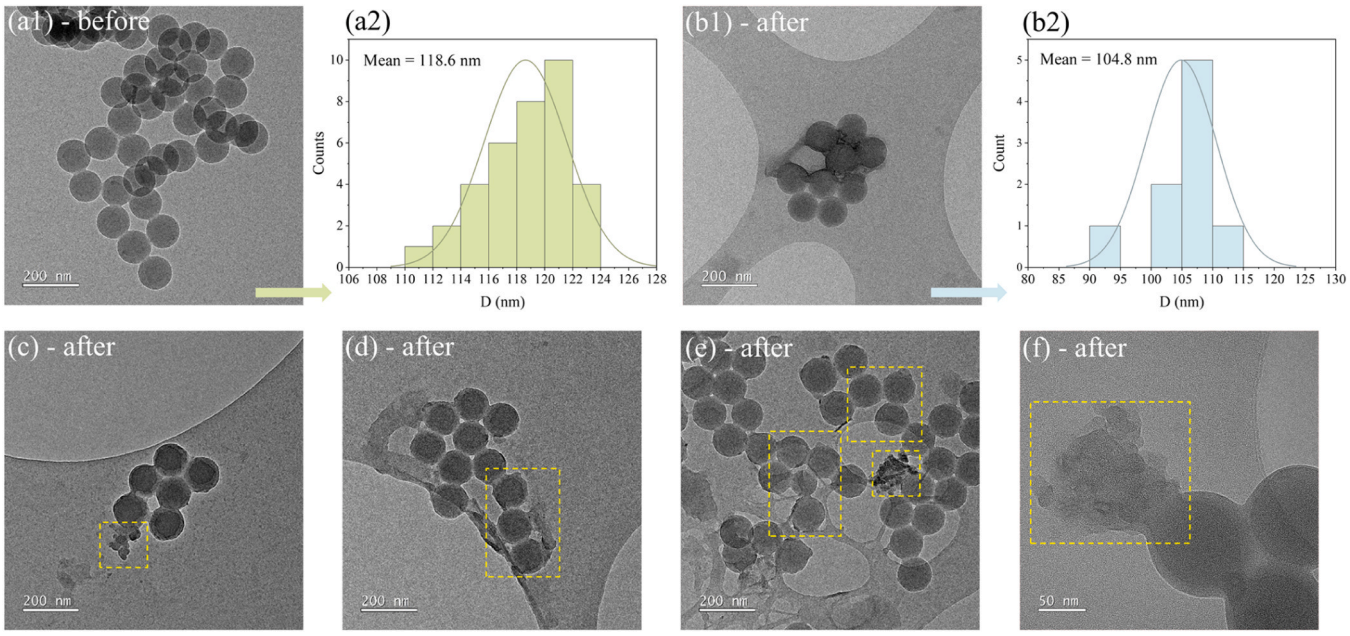

Fig. 6. (a1) and (a2) HRTEM images and size distribution of PS-NPs before reaction; (b1) ~ (f) HRTEM images and size distribution of PS-NPs post-reaction. Conditions: [PS-NPs] = 20 mg/L, pH 7.0, applied current = 20 mA, [Na_2SO_4] = 0.05 mol/L, no aeration.

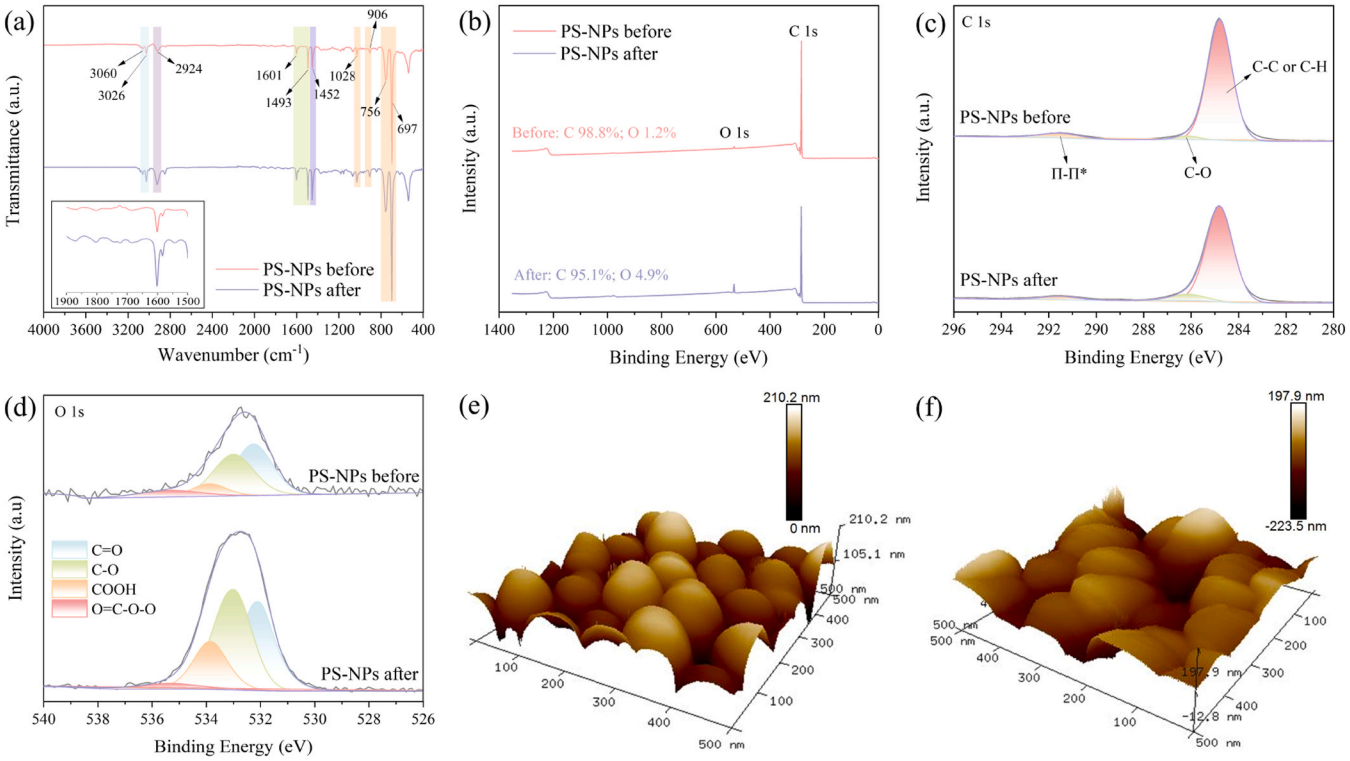

Fig. 7. (a) FTIR spectra; (b) XPS full spectra; (c) C1s XPS spectra; (d) O1s XPS spectra of PS-NPs pre- and post-reaction; (e) AFM topographic image of PS-NPs pre-reaction; and (f) AFM topographic image of PS-NPs post-reaction. Conditions: [PS-NPs] = 20 mg/L; pH 7.0; applied current = 20 mA; [Na_2SO_4] = 0.05 mol/L; no aeration.

was mainly attributed to carboxylic acid, as the COOH peak observed at 533.85 eV in the O1s spectrum increased from 9.59 % to 18.11 %. This finding suggested that oxidation predominantly occurred at the ends of carbon chains, leading to the formation of carboxylic acids.

Topographic images of PS-NPs pre- and post-treatment were obtained using atomic force microscopy (AFM), Fig. 7(e)~(f). The initial particle image showed a relatively organized arrangement of spherical nanoparticles with a consistent height, and the surface profile reflected well-separated nanoparticles with clear boundaries. In comparison, the boundaries between post-reaction PS-NPs particles were less distinct (some overlapping or fusion was observed), and the surface appeared more uneven, suggesting surface erosion and enhanced aggregation post-reaction. Combined with the results from XPS, it is speculated that changes in surface properties, for example, the introduction of oxygen-

containing functional groups, might have enhanced inter-particle interactions resulting in aggregation.

The above analyses characterized the physical deformation and chemical compositional changes in PS-NPs. The electro-Fenton treatment accelerated the formation of plastic fragments and a reduction in particle size. The attack of hydroxyl radicals led to the opening of the benzene ring, and the volatization of small phenyl group-containing molecules on the main polystyrene chain. At the same time, the incorporation of carbonyl groups was enhanced, which was manifested as an increase in the oxidation degree on the polystyrene surface.

3.3. Mechanisms of electrochemical degradation of PS-NPs

3.3.1. DFT calculation and PS-NPs degradation pathways

To further investigate the structural changes of the polystyrene molecules during degradation in the CuCo-CA EF system, DFT (density functional theory) calculations were conducted. Sites with higher f^- and f^0 values exhibit greater reactivity, as they are more susceptible to being attacked by electrophiles and reactive radicals, respectively [46,47]. Accordingly, three styrene monomers were used to analyze the highest occupied molecular orbital (HOMO), and the lowest unoccupied molecular orbital (LUMO) distributions, and to calculate the Fukui index (f^- and f^0 values) based on the natural population analysis (NPA) charge distribution of polystyrene molecules, as given in Fig. 8(a), Figure S8, and Table S1. It was observed that the HOMO was primarily localized around the carbon atoms of the benzene ring, where the electron density is relatively high, making these sites more susceptible to oxidation reactions [48].

For further elucidation of the degradation pattern of polystyrene, optimized polystyrene structures and corresponding reactive sites were labelled with atoms showing relatively high f^- and f^0 values, circled in red, Fig. 8(b). Several reactive sites were observed on the benzene ring of each monomer, indicating that the carbon atoms in the aromatic ring are preferentially attacked. This finding aligned with previously reported observations that hydroxyl radicals preferentially target aromatic rings and double bonds over alkanes [41]. Additionally, carbon atoms on the main chain connecting the benzene rings were also reactive for substitution reactions because the connected hydrogen atoms have a relatively high f^- value.

To clarify the degradation pathway of PS-NPs in the CuCo-CA EF reaction, intermediates were analyzed by direct injection into a mass spectrometer. Figure S9 displays the mass spectrum of the fragmented intermediates, and Table S2 lists the detected degradation products and their structural information. Based on intermediate identification and predicted reaction sites, a potential degradation pathway for PS-NPs was proposed, as shown in Fig. 9. Initially, for hydroxylation on the aromatic ring, atoms with high f^0 values (31 C, 32 C, 42 C, and 43 C) in polystyrene molecule were prone to attack by ·OH radicals, forming hydroxylated intermediates TP5/TP6 ($C_{17}H_{20}O_4$) [15]. The ·OH radicals further attack the polystyrene backbone, preferentially targeting hydrogen atoms along the connecting polymer chain, such as 2 H with a high f^- value of 0.02543, and continue to hydroxylate carbon atoms connected to the benzene ring, forming two isomers TP7/TP8 ($C_8H_{10}O_3$). Subsequent oxidation of these intermediates at the benzene and phenethyl positions leads to the formation of acetophenone (TP9, C_8H_8O) and benzoic acid (TP10, $C_7H_6O_2$). Another pathway observed for TP5/TP6 involved ring-opening reactions on the benzene ring, yielding aliphatic chain compounds such as esters, aldehydes, and alcohols (TP11, TP12, TP13, TP14) [15].

Moreover, due to the electron cloud effects of the benzene ring, carbon atoms connected to the ring exhibit a particle electron-deficient state. Thus, free radicals may initially target the carbon on the polymer chain connected to the benzene ring, breaking C-C bonds in the main chain and resulting in shorter-chain polymers such as TP1/TP2 [49]. Tertiary carbon sites in TP1/TP2 were further attacked by ·OH, yielding smaller fragments of TP3/TP4 ($C_{10}H_{12}O$). Further reactions led to a breakdown of the polystyrene backbone or aromatic ring into lower molecular weight species, including TP15 and TP16, which often contained oxygenated functional groups. The detection of benzoic acid (TP10), 2-butanone (TP16), and polyhydroxylated intermediates (TP13–TP15) suggests extensive oxidation of aromatic rings into small carboxylic and ketonic acids, typical of advanced oxidative degradation. After 6 h of reaction, TOC removal efficiency in the suspension reached 73.7 %, Fig. 1(c). PS-NPs may completely mineralize into CO_2 and H_2O with extended treatment time.

3.3.2. Acute toxicity estimation and proposed mechanism

The acute toxicity of styrene monomers and intermediates formed during the electrochemical degradation process was assessed using the Toxicity Estimation Software Tool (T.E.S.T.), as shown in Table S3 and Fig. 10. The fathead minnow LC_{50} (96) was calculated as 6.09 mg/L for polystyrene, an indication that it is classified as a “toxic” substance (Fig. 10(a)) [50]. Although some intermediates (TP1, TP2, TP5, and TP11) exhibited higher toxicity than styrene, the final products, TP15 and TP16, generated after further electrochemical oxidation, showed a substantial reduction in acute toxicity and were considered “not harmful”. Additionally, Tetrahymena pyriformis IGC_{50} indicates the concentration of a test chemical (mg/L) causing 50 % inhibition after 48 h; the higher the IGC_{50} value, the lower the growth inhibition effect. As illustrated in Fig. 10(b), six intermediates were found to have higher IGC_{50} values than styrene, especially the initial degradation products TP1 and TP2. However, after ring-opening and chain-breaking reactions, growth inhibition significantly decreased. These results demonstrate that while polystyrene decomposition may initially produce more “toxic” intermediates, the reactive oxygen species generated by the CuCo-CA EF system effectively destroy these structures, achieving greater oxidation or mineralization and ensuring post-treatment water safety.

The partially oxidized intermediates identified in this study, such as benzoic acid, hydroxyketones, and polyhydroxylated intermediates,

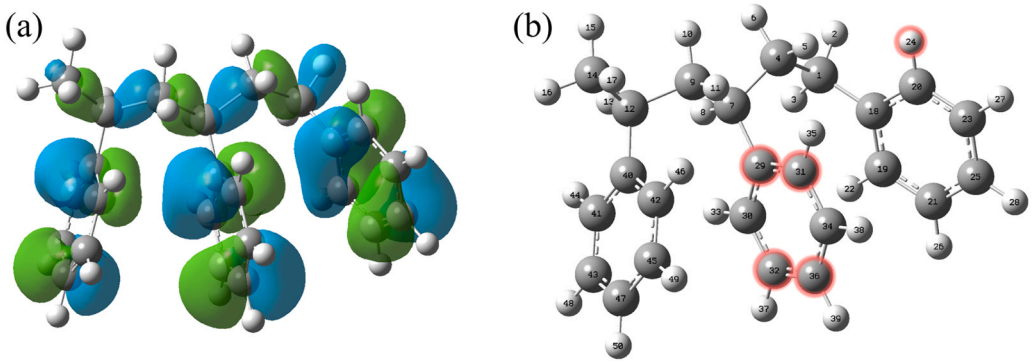

Fig. 8. (a) HOMO distribution map of the polystyrene molecule; (b) Chemical structure and reactive sites on the polystyrene molecule.

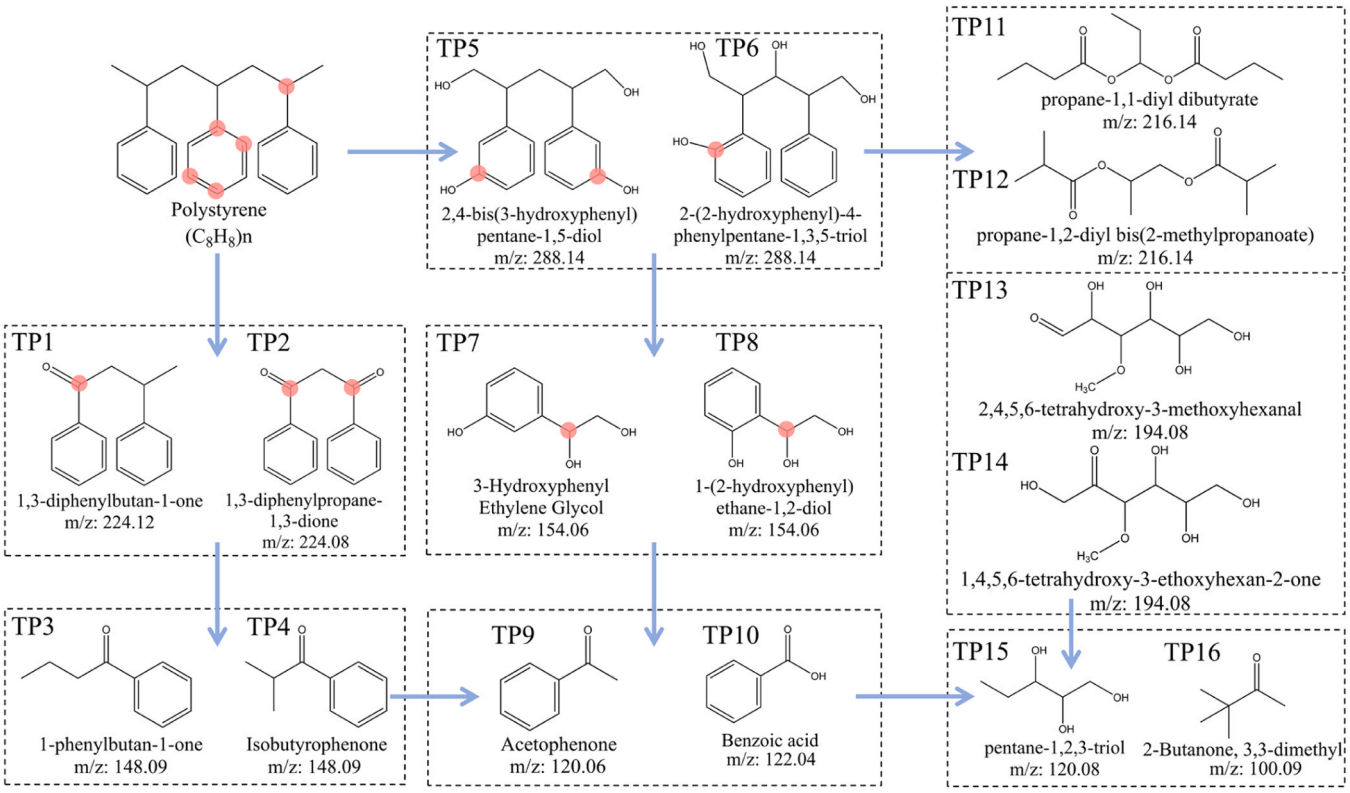

Fig. 9. Degradation pathways of PS-NPs in the CuCo-CA EF system.

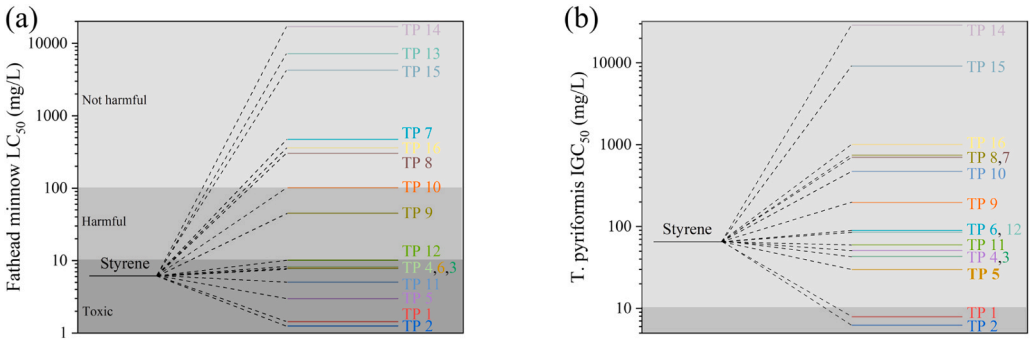

Fig. 10. Acute toxicity estimation of styrene and degradation intermediates.

represent more polar and biodegradable species compared to the parent styrene. Toxicity prediction using T.E.S.T. shows that many of these products are significantly less harmful to aquatic organisms than styrene, with several falling into the 'not harmful' category. TOC measurements further reveal that 73.7 % of the total carbon was mineralized, with the remaining 26.3 % likely corresponding to these low-toxicity intermediates. This highlights the environmental relevance of the CuCo-CA EF treatment in transforming persistent polymers into less hazardous species.

Based on the above findings, the reaction mechanism of PS-NPs degradation in the CuCo-CA EF system can be summarized in Fig. 11. Initially, oxygen evolution (Eq. 9) occurred near the anode, as evidenced by bubble formation, a decrease in solution pH (from 7.01 to 3.35), and an increase in dissolved oxygen concentration (from 8.75 to 13.72 mg/L) during the reaction; our previous study elaborated on this mechanism [23]. The H^+ ions produced during the reaction created a favorable pH environment for *in situ* generation and activation of H_2O_2, as shown in Eq. 3 and Eq. 8. The generated oxygen subsequently diffused to the electrolyte-cathode interface, where it underwent a two-electron reduction pathway to produce H_2O_2. Furthermore, catalytically active Cu(I) and Co(II) sites on the CuCo-CA cathode induced H_2O_2 *in situ* activation, generating highly reactive ·OH free radicals, thereby enabling the oxidative degradation of PS-NPs and step-by-step mineralization.

$$2H_2O \rightarrow 4e^- + 4H^+ + O_2 \quad (9)$$

4. Conclusion

This study proposed an advanced electro-Fenton strategy assisted by a CuCo-CA bifunctional cathode for the treatment of polystyrene nanoplastics (PS-NPs), examining its degradation performance and underlying mechanisms. In this approach, reactive free radicals (·OH) were effectively produced *via* the *in situ* generation and activation of H_2O_2 without the need for external aeration, potentially making it cost-effective at scale. The CuCo-CA EF system achieved a reaction rate constant of 0.4906 h^{-1} for PS-NPs removal at a current density of 4.44 mA/cm^2 and a neutral pH condition, demonstrating improved

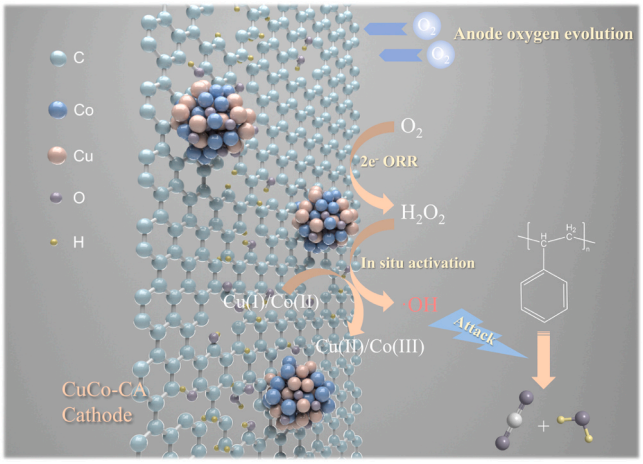

Fig. 11. Schematic of proposed mechanism of PS-NPs degradation in the CuCo-CA EF process.

efficiency compared to EF processes using Cu-CA, Co-CA, or pure CA as the cathode. CuCo-CA exhibited good recyclability over five consecutive runs. The characterization analysis highlighted the physical deformation and chemical composition changes of PS-NPs during electro-Fenton treatment. New surface functional groups were formed as a result of polymer chain fragmentation induced by the oxidative attack of radicals, leading to a loss of spherical shape, size reduction, and particle agglomeration due to surface adhesion. Hydroxyl radicals predominantly attacked the aromatic rings and the carbon atoms on the main chain connected to the benzene rings, causing the incorporation of carbonyl groups and oxidation on the polystyrene surface. After six hours of treatment, TOC removal efficiency in the suspension reached 73.7 %. Reactive radicals effectively degraded potentially more toxic intermediates, gradually mineralizing them into harmless end products, thereby ensuring treated water safety. Overall, this study demonstrates that the CuCo-CA EF process is a promising technology for small-scale nanoplastic treatment in wastewater. Further research could explore its applicability to the degradation of other types of nanoplastics.

CRediT authorship contribution statement

Qian Ye: Writing – original draft, Visualization, Methodology, Investigation, Funding acquisition, Formal analysis, Data curation, Conceptualization. **Hao Xu:** Writing – review & editing, Visualization, Validation, Software, Methodology. **Kale Girish:** Writing – review & editing, Supervision, Resources, Methodology. **Tillotson Martin:** Writing – review & editing, Supervision, Project administration, Investigation, Funding acquisition, Conceptualization. **Hunter Timothy:** Writing – review & editing, Supervision, Resources, Conceptualization. **David Harbottle:** Writing – review & editing, Supervision, Resources, Methodology.

Declaration of Competing Interest

The authors declare that they have no known competing financial interests or personal relationships that could have appeared to influence the work reported in this paper.

Acknowledgements

Qian Ye is funded by the China Scholarship Council (CSC, 202106240065) under the Ministry of Education of P.R. China. The authors are grateful to the funders and acknowledge their support of this work. The authors wish to express their gratitude to colleagues at the University of Leeds who have provided laboratory apparatus, technical support, and training: Mr. Stuart King (FTIR), Dr. Jeanine Williams (HPLC), Dr. Chhaya Patole (MS), and Dr. Ben Douglas (DLS). Additionally, we would like to thank Dr. David Elliott, Mr. Morgan McGowan, and Ms. Emma Tidswell for their guidance on the safe setup and operation of equipment.

Appendix A. Supporting information

Supplementary data associated with this article can be found in the online version at doi:10.1016/j.jece.2025.118907.

Data availability

Data will be made available on request.

References

[1] X. Liang, J. Ye, R. Cao, J. Shuai, J. Zhang, R. Aimaiti, S. Meng, K. Wang, A. Gomiero, J. Wang, W. Wang, J. Yang, Microplastics and their interaction with microorganisms in bosten lake water, J. Clean. Prod. 481 (2024) 144157, https://doi.org/10.1016/j.jclepro.2024.144157.
[2] A.L. Andrady, The plastic in microplastics: a review, Mar. Pollut. Bull. 119 (2017) 12–22, https://doi.org/10.1016/j.marpolbul.2017.01.082.
[3] R. Ahmed, A.K. Hamid, S.A. Krebsbach, J. He, D. Wang, Critical review of microplastics removal from the environment, Chemosphere 293 (2022) 133557, https://doi.org/10.1016/j.chemosphere.2022.133557.
[4] W. Li, J. Hu, Q. Shao, T. Tang, J. Huo, J. Sun, K. Dai, High-performance amino-crosslinked phosphorylated microcrystalline cellulose/MoS_2 hybrid aerogel for polystyrene nanoplastics removal from aqueous environments, J. Colloid Interface Sci. 684 (2025) 457–468, https://doi.org/10.1016/j.jcis.2025.01.047.
[5] Y. Pico, A. Alfarhan, D. Barcelo, Nano- and microplastic analysis: focus on their occurrence in freshwater ecosystems and remediation technologies, TrAC Trends Anal. Chem. 113 (2019) 409–425, https://doi.org/10.1016/j.trac.2018.08.022.
[6] L. Hou, D. Kumar, C.G. Yoo, I. Gitsov, E.L.-W. Majumder, Conversion and removal strategies for microplastics in wastewater treatment plants and landfills, Chem. Eng. J. 406 (2021) 126715, https://doi.org/10.1016/j.cej.2020.126715.
[7] Z. Chen, W. Wei, X. Liu, B.-J. Ni, Emerging electrochemical techniques for identifying and removing micro/nanoplastics in urban waters, Water Res. 221 (2022) 118846, https://doi.org/10.1016/j.watres.2022.118846.
[8] M.C. Krueger, H. Harms, D. Schlosser, Prospects for microbiological solutions to environmental pollution with plastics, Appl. Microbiol. Biotechnol. 99 (2015) 8857–8874, https://doi.org/10.1007/s00253-015-6879-4.
[9] P. Duan, Y. Qi, S. Feng, X. Peng, W. Wang, Y. Yue, Y. Shang, Y. Li, B. Gao, X. Xu, Enhanced degradation of clothianidin in peroxymonosulfate/catalyst system via core-shell FeMn @ N-C and phosphate surrounding, Appl. Catal. B Environ. 267 (2020) 118717, https://doi.org/10.1016/j.apcatb.2020.118717.
[10] M. Kiendrebeogo, M.R. Karimi Estahbanati, A. Khosravanipour Mostafazadeh, P. Drogui, R.D. Tyagi, Treatment of microplastics in water by anodic oxidation: a case study for polystyrene, Environ. Pollut. 269 (2021) 116168, https://doi.org/10.1016/j.envpol.2020.116168.
[11] M. Kiendrebeogo, M.R. Karimi Estahbanati, Y. Ouarda, P. Drogui, R.D. Tyagi, Electrochemical degradation of nanoplastics in water: analysis of the role of reactive oxygen species, Sci. Total Environ. 808 (2022) 151897, https://doi.org/10.1016/j.scitotenv.2021.151897.
[12] Z. Wang, M. Liu, F. Xiao, G. Postole, H. Zhao, G. Zhao, Recent advances and trends of heterogeneous electro-Fenton process for wastewater treatment-review, Chin. Chem. Lett. 33 (2022) 653–662, https://doi.org/10.1016/j.cclet.2021.07.044.
[13] F. Miao, Y. Liu, M. Gao, X. Yu, P. Xiao, M. Wang, S. Wang, X. Wang, Degradation of polyvinyl chloride microplastics via an electro-Fenton-like system with a TiO_2/graphite cathode, J. Hazard. Mater. 399 (2020) 123023, https://doi.org/10.1016/j.jhazmat.2020.123023.
[14] Q. Chen, L. Wan, H. Zhou, F. Luo, L. Lei, N. Wang, Photoelectro-Fenton microreactor integrated with MOF-derived porous α-Fe_2O_3 film for efficient nanoplastics degradation, J. Water Process Eng. 56 (2023) 104343, https://doi.org/10.1016/j.jwpe.2023.104343.
[15] J. Lu, R. Hou, Y. Wang, L. Zhou, Y. Yuan, Surfactant-sodium dodecyl sulfate enhanced degradation of polystyrene microplastics with an energy-saving electrochemical advanced oxidation process (EAOP) strategy, Water Res. 226 (2022) 119277, https://doi.org/10.1016/j.watres.2022.119277.
[16] Q. Ye, T.N. Hunter, H. Xu, D. Harbottle, G.M. Kale, M.R. Tillotson, CuCo carbon aerogel as a bifunctional cathode for electro-Fenton processes: unveiling synergistic effects and catalytic mechanisms, Sep. Purif. Technol. 361 (2025) 131597, https://doi.org/10.1016/j.seppur.2025.131597.
[17] Z. Chen, Z. Huang, J. Liu, E. Wu, Q. Zheng, L. Cui, Phase transition of Mg/Al-flocs to Mg/Al-layered double hydroxides during flocculation and polystyrene nanoplastics removal, J. Hazard. Mater. 406 (2021) 124697, https://doi.org/10.1016/j.jhazmat.2020.124697.
[18] Z. Chen, J. Liu, C. Chen, Z. Huang, Sedimentation of nanoplastics from water with Ca/Al dual flocculants: characterization, interface reaction, effects of ph and ion ratios, Chemosphere 252 (2020) 126450, https://doi.org/10.1016/j.chemosphere.2020.126450.

[19] G. Zhou, X. Huang, H. Xu, Q. Wang, M. Wang, Y. Wang, Q. Li, Y. Zhang, Q. Ye, J. Zhang, Removal of polystyrene nanoplastics from water by CuNi carbon material: the role of adsorption, Sci. Total Environ. 820 (2022) 153190, https://doi.org/10.1016/j.scitotenv.2022.153190.
[20] M. Frisch, G. Trucks, H. Schlegel, G. Scuseria, M. Robb, J. Cheeseman, G. Scalmani, V. Barone, G. Petersson, H. Nakatsuji, Chem. Chem. Phys. Accept. Manuscr. 37 (1988) 785–789. Gaussian 09, revision A. 02, Gaussian, inc., wallingford, CT, 2016.
[21] A.D. Becke, Density-functional thermochemistry. Iii. the role of exact exchange, J. Chem. Phys. 98 (1993) 5648–5652, https://doi.org/10.1063/1.464913.
[22] R.G. Parr, W. Yang, Density functional approach to the frontier-electron theory of chemical reactivity, J. Am. Chem. Soc. 106 (1984) 4049–4050, https://doi.org/10.1021/ja00326a036.
[23] Q. Ye, T.N. Hunter, H. Xu, D. Harbottle, G.M. Kale, M.R. Tillotson, Synergistic effect of fe and ni on carbon aerogel for enhanced oxygen reduction and H_2O_2 activation in electro-Fenton process, Sep. Purif. Technol. 353 (2025) 128436, https://doi.org/10.1016/j.seppur.2024.128436.
[24] Q. Zhang, M. Zhou, X. Du, P. Su, W. Fu, G. Song, Highly efficient dual-cathode Electro-Fenton process without aeration at a wide ph range: simultaneously enhancing Fe(II) regeneration and mineralization efficiency, Chem. Eng. J. 429 (2022) 132436, https://doi.org/10.1016/j.cej.2021.132436.
[25] H. He, Z. Zhou, Electro-Fenton process for water and wastewater treatment, Crit. Rev. Environ. Sci. Technol. 47 (2017) 2100–2131, https://doi.org/10.1080/10643389.2017.1405673.
[26] Y.-C. Kao, Y.-J. Shih, C.-P. Huang, The role of reversible and polarizable surface charge in the electro-sorption of NaCl electrolyte onto activated carbon-graphite electrode, Chem. Eng. J. 430 (2022) 132862, https://doi.org/10.1016/j.cej.2021.132862.
[27] V. Kavitha, K. Palanivelu, Destruction of cresols by fenton oxidation process, Water Res. 39 (2005) 3062–3072, https://doi.org/10.1016/j.watres.2005.05.011.
[28] B. Hou, H. Han, S. Jia, H. Zhuang, P. Xu, K. Li, Three-dimensional heterogeneous electro-Fenton oxidation of biologically pretreated coal gasification wastewater using sludge derived carbon as catalytic particle electrodes and catalyst, J. Taiwan Inst. Chem. Eng. 60 (2016) 352–360, https://doi.org/10.1016/j.jtice.2015.10.032.
[29] M. Teymori, H. Khorsandi, A.A. Aghapour, S.J. Jafari, R. Maleki, Electro-Fenton method for the removal of malachite Green: effect of operational parameters, Appl. Water Sci. 10 (2019) 39, https://doi.org/10.1007/s13201-019-1123-5.
[30] K. Yin, L. Hao, G. Li, CuO nanosheets incorporated scrap steel slag coupled with persulfate catalysts for high-efficient degradation of sulfonamide from water, Environ. Res. 216 (2023) 114614, https://doi.org/10.1016/j.envres.2022.114614.
[31] F.C. Ruiz, P.S. Martínez, E.B. Castro, R. Humana, H.A. Peretti, A. Visintin, Effect of electrolyte concentration on the electrochemical properties of an AB5-type alloy for Ni/MH batteries, Int. J. Hydrog. Energy 38 (2013) 240–245, https://doi.org/10.1016/j.ijhydene.2012.10.007.
[32] L. Wang, J. Jiang, J. Ma, S. Pang, T. Zhang, A review on advanced oxidation processes homogeneously initiated by copper(II), Chem. Eng. J. 427 (2022) 131721, https://doi.org/10.1016/j.cej.2021.131721.
[33] Q. Yang, C. Xia, S. Chen, X. Cao, J. Hao, Enhanced activation of H_2O_2 by bimetallic Cu_2SnS_3: a new insight for cu (II)/Cu (I) redox cycle promotion, J. Colloid. Interface Sci. 640 (2023) 750–760, https://doi.org/10.1016/j.jcis.2023.02.159.
[34] W. Xi, H. Zhou, P. Yang, H. Huang, J. Tian, M. Ratova, D. Wu, Pulse manipulation on Cu-based catalysts for electrochemical reduction of CO_2, ACS Catal. 14 (2024) 13697–13722, https://doi.org/10.1021/acscatal.4c03513.
[35] Y. Li, H. Dong, J. Xiao, L. Li, J. Dong, D. Huang, J. Deng, Ascorbic acid-enhanced CuO/percarbonate oxidation: insights into the pH-dependent mechanism, ACS EST Eng. 3 (2023) 798–810, https://doi.org/10.1021/acsestengg.2c00410.
[36] H. Zhao, X. Shen, Y. Chen, S.-N. Zhang, P. Gao, X. Zhen, X.-H. Li, G. Zhao, A COOH-terminated nitrogen-doped carbon aerogel as a bulk electrode for completely selective two-electron oxygen reduction to H_2O_2, Chem. Commun. 55 (2019) 6173–6176, https://doi.org/10.1039/C9CC02580D.
[37] E. Yousif, R. Haddad, Photodegradation and photostabilization of polymers, especially polystyrene: review, SpringerPlus 2 (2013) 398, https://doi.org/10.1186/2193-1801-2-398.
[38] R. Betancourt-Galindo, C. Cabrera Miranda, B.A. Puente Urbina, A. Castañeda-Facio, S. Sánchez-Valdés, J. Mata Padilla, L.A. García Cerda, Y.A. Perera, O. S. Rodríguez-Fernández, Encapsulation of silver nanoparticles in a polystyrene matrix by miniemulsion polymerization and its antimicrobial activity, Int. Sch. Res. Not. 2012 (2012) 186851, https://doi.org/10.5402/2012/186851.
[39] L.P. Domínguez-Jaimes, E.I. Cedillo-González, E. Luévano-Hipólito, J.D. Acuña-Bedoya, J.M. Hernández-López, Degradation of primary nanoplastics by photocatalysis using different anodized TiO_2 structures, J. Hazard. Mater. 413 (2021) 125452, https://doi.org/10.1016/j.jhazmat.2021.125452.
[40] D. lal S, S.J. T, R. C, Solid-phase photodegradation of polystyrene by nano TiO_2 under ultraviolet radiation, Environ. Nanotechnol. Monit. Manag. 12 (2019) 100229, https://doi.org/10.1016/j.enmm.2019.100229.
[41] D. Ortiz, M. Munoz, J. Nieto-Sandoval, C. Romera-Castillo, Z.M. de Pedro, J. A. Casas, Insights into the degradation of microplastics by fenton oxidation: from surface modification to mineralization, Chemosphere 309 (2022) 136809, https://doi.org/10.1016/j.chemosphere.2022.136809.
[42] P. Liu, L. Qian, H. Wang, X. Zhan, K. Lu, C. Gu, S. Gao, New insights into the aging behavior of microplastics accelerated by advanced oxidation processes, Environ. Sci. Technol. 53 (2019) 3579–3588, https://doi.org/10.1021/acs.est.9b00493.
[43] M.L. Goodson, R. Lagle, P. Guggilla, X-Ray photoelectron spectroscopy of polystyrene composite films, J. Adv. Mater. Sci. Eng. 2 (2022), https://doi.org/10.33425/2771-666X.1007.
[44] X. Chen, X. Wang, D. Fang, A review on C1s XPS-spectra for some kinds of carbon materials, Fuller. Nanotub. Carbon Nanostruct. 28 (2020) 1048–1058, https://doi.org/10.1080/1536383X.2020.1794851.
[45] Y. Yang, J. Chen, Z. Chen, Z. Yu, J. Xue, T. Luan, S. Chen, S. Zhou, Mechanisms of polystyrene microplastic degradation by the microbially driven fenton reaction, Water Res. 223 (2022) 118979, https://doi.org/10.1016/j.watres.2022.118979.
[46] W. Guo, Q. Zhao, J. Du, H. Wang, X. Li, N. Ren, Enhanced removal of sulfadiazine by sulfidated ZVI activated persulfate process: performance, mechanisms and degradation pathways, Chem. Eng. J. 388 (2020) 124303, https://doi.org/10.1016/j.cej.2020.124303.
[47] M. Tong, F. Liu, Q. Dong, Z. Ma, W. Liu, Magnetic Fe_3O_4-deposited flower-like MoS_2 nanocomposites for the Fenton-like escherichia coli disinfection and diclofenac degradation, J. Hazard. Mater. 385 (2020) 121604, https://doi.org/10.1016/j.jhazmat.2019.121604.
[48] S. Mao, C. Liu, Y. Wu, M. Xia, F. Wang, Porous P, Fe-doped g-C_3N_4 nanostructure with enhanced photo-Fenton activity for removal of tetracycline hydrochloride: mechanism insight, DFT calculation and degradation pathways, Chemosphere 291 (2022) 133039, https://doi.org/10.1016/j.chemosphere.2021.133039.
[49] Y. Cai, F. Chen, L. Yang, L. Deng, Z. Shi, Degradation of polystyrene nanoplastics in UV/NaClO and UV/PMS systems: insights into degradation efficiency, mechanism, and toxicity evaluation, Water 15 (2023) 1920, https://doi.org/10.3390/w15101920.
[50] Z. Cai, X. Hao, X. Sun, P. Du, W. Liu, J. Fu, Highly active WO_3@anatase-SiO_2 aerogel for solar-light-driven phenanthrene degradation: mechanism insight and toxicity assessment, Water Res. 162 (2019) 369–382, https://doi.org/10.1016/j.watres.2019.06.017.